








Two-Dimensional Numerical Study of the Transient Flow Conditions in Complete Shock Tunnel

A.M. Mohsen¹, M.Z. Yusoff², Hakim S. Sultan Aljibori¹ A. Al-Falahi³,
Abdul Amir H. Kadhum⁴

¹ Department of Air-conditioning and Refrigeration Techniques Engineering, University of Warith Al-Anbiyaa, Karbalaa- Baghdad Rd, 56001, Iraq, Email: alimmohsen@uowa.edu.iq

² Centre of Advanced Computational Engineering, College of Engineering, Universiti Tenaga Nasional, Jalan IKRAM-UNITEN, 43000 Kajang, Selangor, Darul Ehsan, Malaysia, Email: zamri@uniten.edu.my

³ Sheridan College, Davis Campus, 7899 McLaughlin Rd., Brampton, ON, L6Y 5H9, Canada, Email: amir.alfalahi@sheridancollege.ca

⁴ University of Al-Ameed, Karbalaa, Iraq, Email: amir1719@gmail.com

Received October 20 2020; Revised January 15 2021; Accepted for publication January 15 2021.

Corresponding author: A.M. Mohsen (alimmohsen@uowa.edu.iq)

© 2021 Published by Shahid Chamran University of Ahvaz

Abstract. In the current research, an axisymmetric model is developed to study high-speed unsteady flow in the test section of a 7 meter-long shock tunnel. The computational calculations of the shock tunnel are conducted using the Fluent CFD solver. The Finite Volume Method (FVM) is used to discretize the governing equations of mass, momentum, and energy. The accuracy of the numerical model is investigated with first-order upwind, second-order upwind, and third-order MUSCL schemes. Adaptive mesh refinement is implemented to resolve the shock wave and contact surface regions accurately. The numerical results are compared with theoretical calculations and experimental data from experimental tests and the comparison shows good agreement. Different test gases of Helium, Air and CO₂, are utilized in the current study. The results show that steady test conditions are maintained for a longer test time by adjusting the pressure ratio and gas combination across the diaphragm. The highest shock wave speed and strength are achieved for a gas combination of Helium-CO₂, but a longer test duration is observed when using Air as the test gas.

Keywords: Shock tunnel, Supersonic flow, Shock wave, CFD, Mach number.

1. Introduction

The performance of hypersonic and high-speed supersonic vehicles is affected by complex flow conditions. Those conditions include viscous interaction, ionization, thin shock layer, and high total and stagnation temperature [1, 2]. The risk and high cost of building those vehicles precluded experimental flight testing. To overcome this constraint, different ground-based test facilities were developed [3-9]. Among those is the shock tunnel facility [11, 12].

Shock tunnels are of short time and high-speed flow. They can produce gas flow conditions similar to those encountered by supersonic aircraft, as well as atmospheric space re-entry vehicles during their actual flight [13-15]. Studies have shown that flow conditions of Mach numbers ranging from 1.73 to 10 can be achieved in such test facilities [16-18].

However, these conditions can only last for a very short duration, which is in the order of milliseconds [19-22]. Hence, it is challenging to conduct experiments to study some of the flow parameters in such a short time. In contrast, the modeling of such flow is an alternative method to describe the flow procedure and to predict the optimum operation.

Recent research in high-speed flow has demonstrated increased attention on the numerical modeling of shock tube, shock tunnel, and gun tunnel [23-26]. In these studies, the numerical pressure data has been compared with the practical results [27]. Al-Falahi et al. [28-29] developed a new 2D time-accurate model as a numerical Euler solver and evaluated the performance of a new experimental shock tube facility. Further modifications on the solver were performed by Mohsen et al. [30-31] to investigate the area contraction effect on a shock tube performance. Other researchers such as Andreotti et al. [32] introduced a new numerical method using finite element analysis and predicted the dissipation in a shock tube that has a double-diaphragm configuration. They reported that the non-ideal opening of a ruptured diaphragm can cause losses in pressure in the test facility.

Kotov et al. [33] carried out two-dimensional viscous modeling and successfully produced, for the first duration, a realistic and non-equilibrium hypersonic stream that simulates the mock behavior of NASA - electric arc shock tube (EAST). Mundt et al. [34] introduced a new numerical approach, which was developed the quasi-1-D Lagrangian code of Jacobs et al. [25], to simulate different piston-driven shock tunnels. Their method was notified to be ideal or typical for the design process of new ground-based facilities of similar operating conditions.



Table 1. Principle dimensions of test facility.

Zone	Description
Driver section	2500 mm long tube of 50 mm diameter
Driven section	4035 mm long tube of 50 mm diameter
Mach 4 nozzle	Convergent-divergent nozzle with outer diameter of 70 mm, 7 mm throat diameter, and 389 mm as a total length
Test section	324 mm x 304 mm x 304 mm
Dump tank	1 m ³ cubical tank

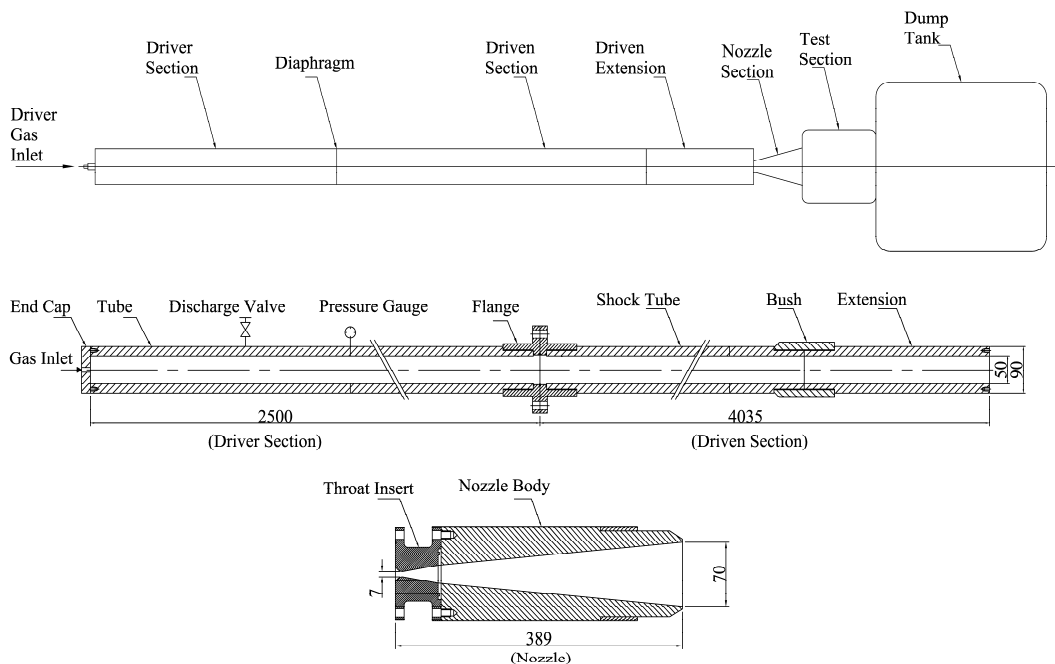
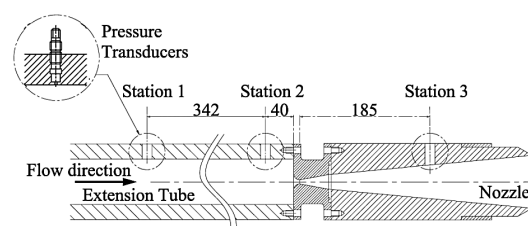
For the development of new high-speed flow short-duration facilities, it is imperative to determine the effects of various parameters such as geometrical and operational impacts on the test conditions for the optimal operation. Such a process is more effective and less costly when carried out numerically. This work aims to develop a numerical model for a full-scale shock tunnel test facility at The University Tenaga Nasional (UNITEN), Malaysia. The developed model is used to study the transient flow behavior in the complete geometry of the shock tunnel to determine optimum operating conditions for the longest possible test duration in the test section.

2. Description of Shock Tunnel

The Experimental pressure history data were recorded from the test facility at UNITEN. A schematic is shown in Fig. 1. The dimensions of the facility are shown in Table 1. The driven and driver tubes are made from different alloys of steel and separated by a primary aluminum diaphragm. The primary diaphragm isolates the driver gas (high-pressure gas) from the test gas in the driven section. Another secondary diaphragm, made from light plastic, was placed before the nozzle section. Before each run, the gases in the test part and the dump tank were discharged to achieve roughly 1 kPa. The desired test gases of Carbon dioxide or air is used to fill the driven tube. Compressed driver gas of Helium or Air is used in the high-pressure tube of the experimental facility.

There are three piezoelectric pressure sensors (Piezo-tronics Inc., type 111A24) were installed near the end of the low pressure tube and on the nozzle (shown in Fig. 2). The sensors were used to report the experimental pressure data during each run.

The axial distance between the first pressure sensor (station 1) and the second sensor (station 2) is 342 mm. Station 2 is 40 mm before the end of the driven tube. The third pressure transducer (station 3) is located on the nozzle at a distance of 185 mm from its throat. Additionally, a static pressure transducer, appointed as station 4, is fixed on the driver part to record the driver pressure P_4 that ruptures the primary diaphragm. To record the flow Mach number, an additional station is chosen and indicated as station 5. Station 5 is in the test section at a distance of 100 mm downstream the nozzle exit of the shock tunnel. All transducers of pressure are linked to a data acquisition device that observes the instantaneous pressure changes and captures the shock wave.

**Fig. 1.** Schematic of shock tunnel.**Fig. 2.** Pressure transducer locations.

3. Numerical Analysis and Modeling

3.1 Controlling Equations

The continuity equation of the two-dimensional axisymmetric model is written as:

$$\frac{\partial \rho}{\partial t} + \frac{\partial(\rho v_x)}{\partial x} + \frac{\partial(\rho v_r)}{\partial r} + \frac{\rho v_r}{r} = 0 \tag{1}$$

The axial and radial momentum conservation equations are given by:

$$\frac{\partial(\rho v_x)}{\partial t} + \frac{1}{r} \frac{\partial(r \rho v_x v_x)}{\partial x} + \frac{1}{r} \frac{\partial(r \rho v_r v_x)}{\partial r} = -\frac{\partial p}{\partial x} + \frac{1}{r} \frac{\partial}{\partial x} \left[r \mu \left(2 \frac{\partial v_x}{\partial x} - \frac{2}{3} (\nabla \cdot \vec{v}) \right) \right] + \frac{1}{r} \frac{\partial}{\partial r} \left[r \mu \left(\frac{\partial v_x}{\partial r} + \frac{\partial v_r}{\partial x} \right) \right] + F_x \tag{2}$$

$$\frac{\partial(\rho v_r)}{\partial t} + \frac{1}{r} \frac{\partial(r \rho v_x v_r)}{\partial x} + \frac{1}{r} \frac{\partial(r \rho v_r v_r)}{\partial r} = -\frac{\partial p}{\partial r} + \frac{1}{r} \frac{\partial}{\partial x} \left[r \mu \left(\frac{\partial v_r}{\partial x} + \frac{\partial v_x}{\partial r} \right) \right] + \frac{1}{r} \frac{\partial}{\partial r} \left[r \mu \left(2 \frac{\partial v_r}{\partial r} - \frac{2}{3} (\nabla \cdot \vec{v}) \right) \right] - 2 \mu \frac{v_r}{r^2} + \frac{2}{3} \frac{\mu}{r} (\nabla \cdot \vec{v}) + \rho \frac{v_r^2}{r} + F_r \tag{3}$$

For viscous flow, the energy transport equation is written as:

$$\frac{\partial(\rho E)}{\partial t} + \nabla \cdot [\vec{v}(\rho E + p)] = \nabla \cdot [k_{eff} \nabla T + (\tau_{eff} \cdot \vec{v})] + S_h \tag{4}$$

3.2 Numerical Scheme

3.2.1 Finite volume Approach

The basic formula of the generic transport equation for the scalar (ϕ) of a control volume (V) can be written:

$$\frac{d}{dt} \int_V \rho \phi dV + \oint \rho \phi \vec{v} \cdot d\vec{A} = \oint \Gamma_\phi \nabla \phi \cdot d\vec{A} + \int_V S_\phi dV \tag{5}$$

Discretizing eq. (5) for a specific cell:

$$\frac{\partial \rho \phi}{\partial t} V + \sum_f^{N_{faces}} \rho_f \phi_f (\vec{v})_f \cdot \vec{A}_f = \sum_f^{N_{faces}} \Gamma_\phi \nabla \phi_f \cdot \vec{A}_f + S_\phi V \tag{6}$$

At the cell center and surrounding neighboring cells, the scalar transport equation (Eq. (6)) has the unknown variable ϕ and linearized by:

$$a_p \phi = \sum_{nb} a_{nb} \phi_{nb} + b \tag{7}$$

3.2.2 Spatial discretization

To capture the shock wave with less oscillation in the solution, the Advection Upstream Splitting Method (AUSM) has been used to produce the accurate resolution of shock discontinuities in high-speed transient stream [35]. To compute the gradient (ϕ) at the cell center (C_0), the following discrete form is used:

$$(\nabla \phi)_c = \frac{1}{V} \sum_f \bar{\phi}_f \vec{A}_f \tag{8}$$

where $\bar{\phi}_f$ is computed as:

$$\bar{\phi}_f = \frac{1}{N_f} \sum_n^{N_f} \bar{\phi}_n \tag{9}$$

3.2.3 Temporal discretization

To perform the time progressing, the first order backward difference equation was used. The derivative of the first part of eq. (5) is written as:

$$\frac{d}{dt} \int_V \rho \phi dV = \frac{(\rho \phi V)^{n+1} - (\rho \phi V)^n}{\Delta t} \tag{10}$$

where, V^{n+1} can be calculated by:

$$V^{n+1} = V^n + \frac{dV}{dt} \Delta t \tag{11}$$

The volume duration derivative of the control volume dV / dt can be calculated by:

$$\frac{dV}{dt} = \int_V u_g \cdot d\vec{A} = \sum_j^{n_f} u_{g,j} \cdot \vec{A}_j \tag{12}$$



The term $u_{g,j} \cdot \vec{A}_j$ is calculated from:

$$u_{g,j} \cdot \vec{A}_j = \frac{\delta V_j}{\Delta t} \quad (12)$$

Equation (11) is solved iteratively at each step. To sustain the time precision of these solutions, the range of time-step starting from 1.0×10^{-6} to 5.0×10^{-6} is used. Within this range, a convergence of 1.0×10^{-4} with iterations of less than 10 was obtained.

3.3 Computational Grid

The numerical model of the shock tunnel was developed according to the dimensions of the whole geometry of the shock tunnel. The flow domain is modeled with an axis-symmetric structured mesh, as shown in Fig. 3.

3.4 Boundary conditions

Only solid boundaries were considered since the stream or flow is restricted within the shock tunnel walls. The no-slip conditions were imposed, and the adiabatic condition was selected for the energy equation. At the facility axis, the axis-symmetry condition was used.

3.5 Mesh refinement study

For the mesh independence study, four levels of refinement of 25000, 50000, 90000, and 135000 nodes were used, and the pressure history in the driven section was captured as shown in Fig. 4. The initial pressure ratio across the primary diaphragm was 10 and Air was the driver and driven gas. Figure 4 shows that the pressure values are independent of the grid size for resolution of 90000 nodes and above.

3.6 The precision of the numerical method

To investigate the precision of the numerical method, the numerical density profiles along the shock tunnel from the 1st order upwind, 2nd order upwind [36], and 3rd order MUSCL [37] schemes were compared with the exact solution of the 1-D shock tunnel theory and depicted in Fig. 5. The figure shows that the shock wave position was predicted well by 1st order scheme, while a small error at the contact surface location was observed. Across the contact surface, the density profile is slightly twisted. However, this smearing effect was reduced when implementing the 2nd order upwind scheme. A similar observation has been made for the 3rd order MUSCL scheme. However, the MUSCL scheme produced an unphysical behavior in the solution upstream of the contact surface. The contact surface fluctuated with moving downstream the driven section. This numerical issue is related to the higher-order gradients which led to over-shoots and under-shoots in the density values [38]. Thus, the 2nd order was used in the modeling of the shock tunnel.

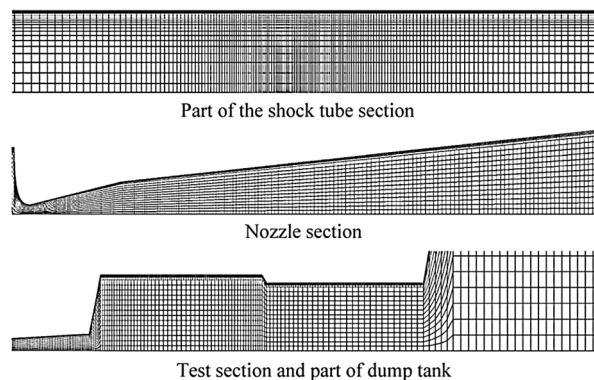


Fig. 3. The axisymmetric mesh generation.

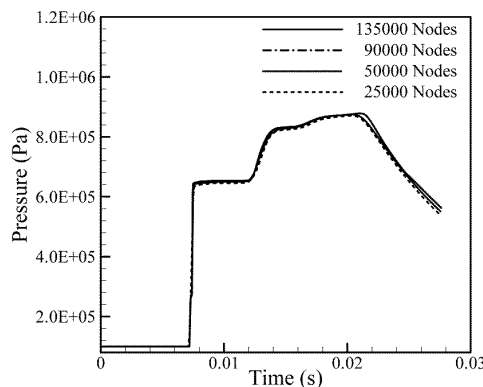


Fig. 4. Pressure history (station 2) for different levels of refinement.



3.7 Turbulence modeling

Boundary layer growth behind the shock wave in the shock tube section of a shock tunnel has a significant influence on flow parameters such as shock wave strength, gas density, and test duration [39, 40]. To ensure that those effects are captured accurately, various turbulence models such as the Realizable and RNG $k-\epsilon$, $k-\omega$, and the Reynolds Stress Model (RSM) on the flow variables in the shock tunnel were examined. The S.S.T $k-\omega$ and RSM caused an increase in the computational results. However, all turbulence models have shown independent behavior on the numerical data. Since the Realizable $k-\epsilon$ model gives reliable results for flow that includes boundary layers under intensive pressure gradients and produces low-cost calculation, this model was selected. The mesh near the boundary was generated carefully by maintaining a value of y^+ close to 1 and less than 5.

3.8 Experimental and numerical Comparison

For validation, numerical simulations are compared to available experimental data from the shock tunnel, the calculations were conducted in the driver pressure range of 1000 kPa, driven pressure of 100 kPa, and dump tank pressure maintained at atmospheric level. Figure 6 compares the numerical and the experimental pressure histories monitored at station 1 and station 2. From this figure, there is a good agreement when predicting the shock wave and reflected shock wave strength and speed. However, over-prediction of total peak pressure is observed. This issue is related to the process of bursting the diaphragm. Practically, the opening of the diaphragm is usually smaller than the diameter of the tube, which causes some blockage to the flow of the high-pressure gas to the driven tube [30, 31]. This process was not accounted for in the CFD calculations as the diaphragm was assumed to be completely removed at $t = 0$.

4. Results and Discussion

The instantaneous pressure history, shock wave speed, and flow Mach number are analyzed at three different sections in the shock tunnel. These sections are the driver tube end (station1 and station 2), nozzle (station 3), and test section (station 4). In the present work, driver-driven gas collection of Helium-Air, Air-Air, and Helium-CO₂ has been chosen to operate the shock tunnel. The shock tunnel operating conditions selected to obtain the following results are tabulated in Table 2.

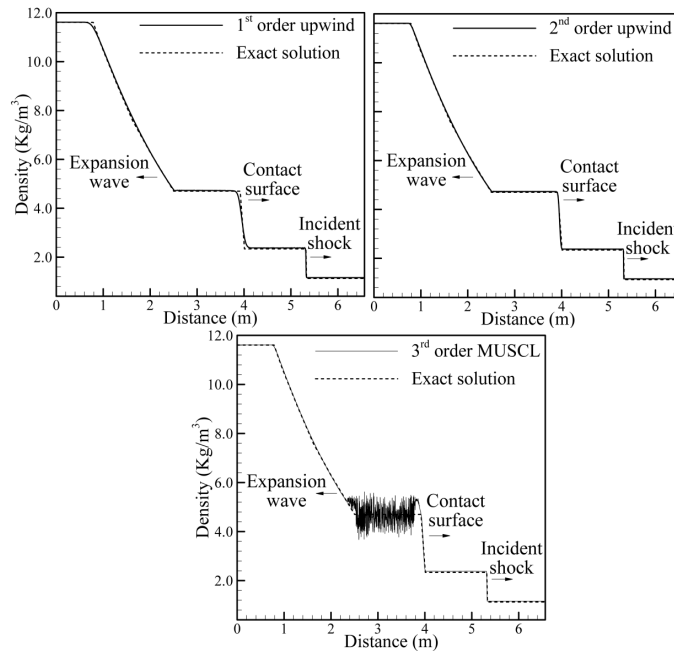


Fig. 5. Density profiles for exact solution compared to 1st, 2nd and 3rd schemes.

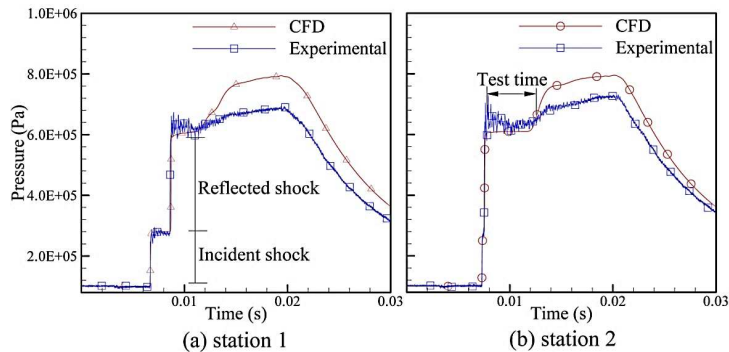


Fig. 6. CFD vs. experimental pressure histories (Air /Air, $P_4 = P_1 = 10$).



Table 2. Operating Conditions for Shock Tunnel.

Parameters	Driver	Driven	Dump Tank
Pressure (bar)	20	1	0.035
Temperature (K)	300	300	300
Gas Type	Run1	Air	Air
	Run2	Helium	Air
	Run3	Helium	Co2

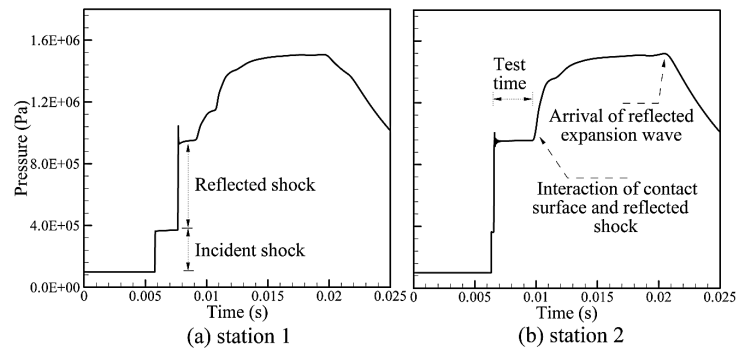
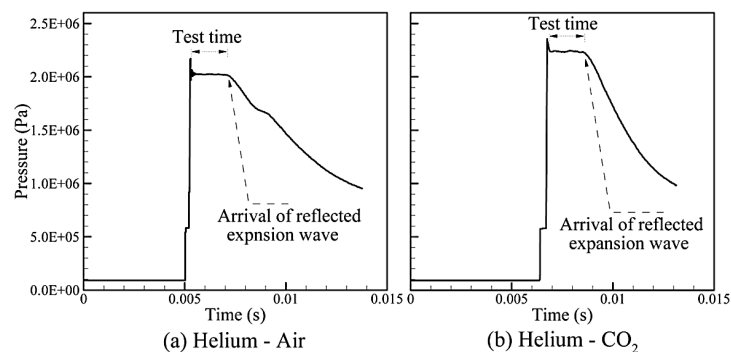
4.1 Pressure History

The instantaneous pressure histories in the driven tube end (station 1 and station 2) for the gas combination of Air-Air and diaphragm pressure ratio of 20 are depicted in Fig. 7. When tracing the pressure history at station 1 (Fig. 7-a), there was a sudden increase from 100 kPa to about 380 kPa after 5.8 ms from diaphragm rupture. This rapid change in pressure represents the arrival of the incident shock wave to the first pressure transducer at station 1. Following that, the incident shock wave reflected off when reaching the driven tube end. The reflected shock wave further heated and compressed the test gas, raising its pressure to 960 kPa. The resultant hot and high-pressure slug of gas in the driven tube end served as a reservoir to supply the nozzle and expanded into the supersonic flow. This process continued until the arrival of the contact surface, which interacted with the reflected shock wave and modified the test gas pressure. As a result, the test time, at which the reservoir pressure in the driven tube end is constant, is found to be around 3.5 ms (Fig. 7-b).

To monitor the pressure histories for different gas combinations, Fig. 8 gathers the recorded pressures in the driven tube end (Station 2) for Helium-Air and Helium-CO₂. Helium-CO₂ provides the best results in term of providing higher nozzle reservoir pressure (test gas pressure) of 2250 kPa, while for Helium-Air is 2000 kPa. However, the test time for both gas combinations is found to be similar (2 ms). The use of low molecular weight gas (Helium) in the driver part helped to improve the performance of the shock tunnel by producing higher speed, stronger shock waves. In contrast, the test time was reduced (compared to Air-Air), as stronger rarefaction waves reflected and travelled back to the driven tube to overtake the reflected shock wave and modified the flow in the nozzle. Therefore, obtaining a longer test time in shock tunnel can be done either by extending the length of the driven section to delay the arrival of the reflected expansion wave or by using a free light piston in the driven section, which is known as a gun tunnel.

4.2 Flow Mach number

The 2-D contour plots for flow Mach number along with the nozzle and facility test section at different selected times for Helium-CO₂ gas combination is shown in Fig. 9. In the shock tunnel, the driver gas pressure is much higher than the driven gas which results in a rapid expansion and shock wave generation after rupturing the diaphragm. As mentioned earlier, the shock wave compresses and heats the driver gas as it propagates downstream the driven tube. In Fig. 9, the shock wave reaches the tube end at time $t = 6.5$ ms from diaphragm rupture. The shock wave then reflects at the nearly closed end of the compression tube, generating other transmitted waves which in turn transverse through the nozzle throat. This process is visualized at time $t = 6.7$ ms. During this time, supersonic test gas flow establishes in the divergent section of the nozzle. The test gas expands through the nozzle, and high-speed flow of about Mach 4.0 is noticed in the test section from time $t = 7.0$ ms until $t = 9.0$ ms.

**Fig. 7.** Instantaneous pressure histories from Air-Air gas combination.**Fig. 8.** Instantaneous pressure histories at driven tube end (station 2) for different gases.

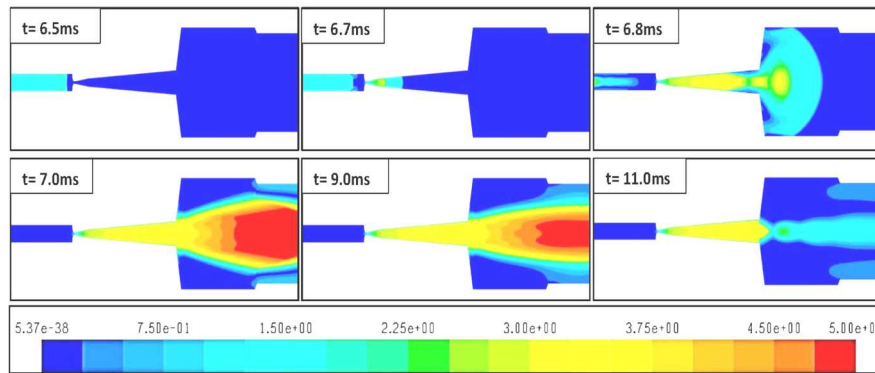


Fig. 9. Contour plots for flow Mach number in nozzle and test section.

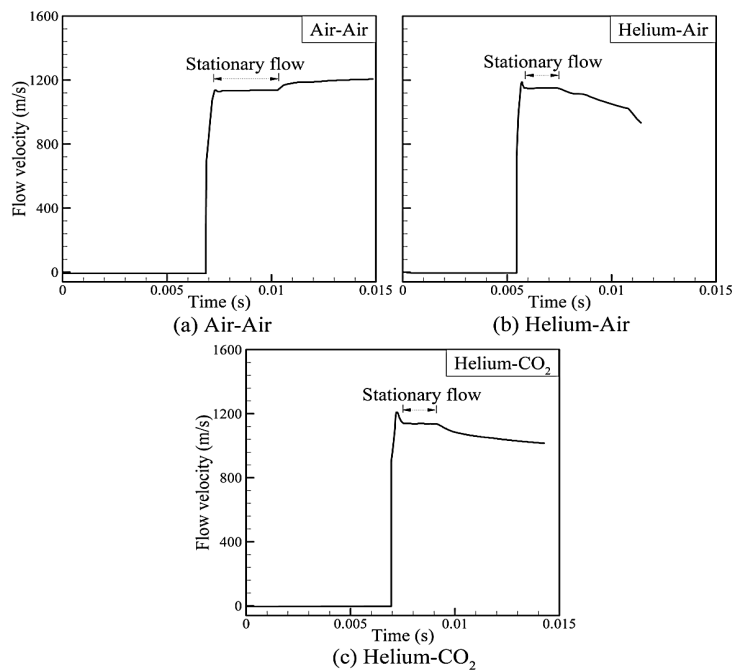


Fig. 10. Flow velocity in the test section (station 4) for different gas combinations.

To determine the “stationary” useful time for aerodynamic testing from different gas combinations, the flow velocity history was observed in the test section (station 4) where a model could be placed as shown in Fig. 10.

Figure 10 introduces the pressure histories for Air-Air, Helium-Air, and Helium-CO₂. Although Helium-CO₂ introduced better results in term of generating stronger shock waves in the driven tube, nozzle design limitation has prevented from producing a higher flow Mach number in the test section (nozzle has a design Mach number of 4.0). For the three different gas combinations, the obtained stationary flow velocity is about 1150 m/s. However, the longest stationary flow for aerodynamic testing is obtained for the gas combination of Air-Air, where steady flow maintained at station 4 as shown in Fig. 10-a. Therefore, the Air-Air gas combination can be considered to provide better results in terms of achieving a longer stationary flow time of about 3.5 ms, when compared to Helium-CO₂ and Helium-Air of less than 2.0 ms.

The test duration of the current shock tunnel configuration is quite comparable to other existing experimental facilities [41 - 44]. Hideyuki et al. [41] conducted an experimental and numerical study in the free-piston high enthalpy shock tunnel HIEST to measure unsteady drag force of a 500mm length HB-2 standard model. The shock tunnel produced stagnation pressures up to 150 Mpa and the test time was ranging from 2 ms to 4 ms. Robinson et al. [42] developed an internal force balance for the High Enthalpy Shock Tunnel Gottingen (HEG) of the German Aerospace Center (DLR). The facility was capable of producing a flow Mach number of 7.8 underflow duration of about 4 ms. Wang et al. [41] conducted a numerical investigation in the nozzle and test section of 265 meters long under Mach 3.9 pressure ratio of about 17.5 and obtained a flow duration of about 4.5 ms as a useful test time. Robinson et al. [44] designed a stress-wave force balance to study a large 1.165 m scramjet model in a reflected shock tunnel that produces Mach 7 and Mach 10. The test time was ranging from 2 to 7 ms.

5. Conclusion

A new numerical model of axis-symmetric shape was developed to study the high-speed transient flow conditions in the test section of 7 meter-long shock tunnel facility. The effects of different gases and pressure ratios on flow velocity and test time were investigated in this article. Computational Fluid Dynamics (CFD) simulations were conducted using an implicit coupled solver with AUSM flux differencing scheme, and the Realizable K-epsilon turbulence model. Three different gases of Air, Helium, and Carbon Dioxide were selected to perform the study. The results show that the two-dimensional computational modeling of the complete flow region of the short duration, the high-speed transient facility is an effective way to understand the flow process involved and to estimate the optimum operating conditions.



It is evident that higher shock wave speed can be achieved when using lighter gas of low molecular weight as the driver gas. The helium-CO₂ gas combination produced the strongest shock wave and the highest test gas pressure among the other gas combinations in the shock tunnel. However, the test time varied distinctively when using different gases. The test time of Helium-CO₂ was very short compared to Air-Air. The arrival of the rarefaction waves reduced the test gas pressure and modified the nozzle flow conditions. The total test time for Helium-CO₂ and similarly for Helium-Air, was less than 2 ms. The longest useful stationary flow for aerodynamic testing in the test section was about 3.5 ms with a flow Mach number of 4.0 when Air is used in the driver and driven sections of the shock tunnel. Accordingly, it is observed that test duration in shock tunnels can be extended by adjusting the type of gases and initial pressure conditions across the primary diaphragm. The implementation of two-dimensional simulation of the unsteady flow in the complete facility helped in obtaining useable data for improving the flow quality and facility performance. Further upgrades to the present design is needed to produce a longer test time for high-speed flow investigation.

Author Contributions

A.M. Mohsen: methodology, developed the numerical modeling, performed the validation, data curation, and visualization, and writing the original draft; M.Z. Yusoff: supervision, conceptualization, methodology, data curation; Hakim S. Sultan Aljibori: reviewing, editing, and investigation; A. Al-Falahi: developing the experimental facility, and obtaining the experimental data. Abdul Amir H. Kadhum: reviewing, editing the final version. The manuscript was written through the contribution of all authors. All authors discussed the results, reviewed, and approved the final version of the manuscript.

Conflict of Interest

The authors declared no potential conflicts of interest concerning the research, authorship, and publication of this article.

Funding

The authors received no financial support for the research, authorship, and publication of this article.

Nomenclature

\vec{A}	Surface area vector [m ²]	N_{faces}	Number of cell faces
a_p, a_{nb}	Linearized coefficients for ϕ and ϕ_{nb} respectively	n_f	Number of faces on the control volume
E	Total energy [J]	P	Static pressure [Pa]
F_x, F_r	External body forces [N]	S_ϕ	Source term of ϕ
k_{eff}	Local thermal conductivity [W/m.k]	V	Cell volume [m ³]
k	Turbulent thermal conductivity [W/m.k]	\vec{v}	Fluid velocity vector [m/s]
k_t	Effective thermal conductivity ($k_{eff} = k + k_t$) [W/m.k]	u_x	Axial velocity [m/s]
N_f	Node number at each face	u_r	Radial velocity [m/s]

Greek symbols

ρ	Density [Kg/m ³]	∇	Gradient
Γ	Diffusion coefficient	$\bar{\phi}_f$	Scalar value at the center of cell face
τ_{eff}	Stress tensor	ϕ	General scalar
δV_j	Volume swept out by the control volume face j over the time step Δt		

Subscripts

eff	Effective	$n + 1$	Respective quantity at the next time step
f	Cell face	r	Radial coordinate
nb	Refers to the neighboring cells	x	Axial coordinate
n	Respective quantity at the current time step		


References


- [1] Peng, Y., Gerdroodbary, M.B., Sheikholeslami, M., Shafee, A., Babazadeh, H., Moradi, R., Mixing enhancement of the multi hydrogen fuel jets by the backward step, *Energy*, 203, 2020, 25438-25451.
- [2] Liu, X., Gerdroodbary, M.B., Sheikholeslami, M., Moradi, R., Shafee, A., Li, Z., Effect of strut angle on performance of hydrogen multi-jets inside the cavity at combustion chamber, *International Journal of Hydrogen Energy*, 45(55), 2020, 31179-31187.
- [3] Nagai, H., Yang, H.S., Ueta, Y., Murakami, M., Takano, N., Yanaka, K., Application of super fluid shock tube facility to experiments of highly transient low-temperature thermo-fluid dynamic phenomena, *Cryogenics*, 41(5-6), 2001, 421-428.
- [4] Buttsworth, D., Jones, T., High bandwidth stagnation temperature measurements in a Mach 6 gun tunnel flow, *Experimental Thermal and Fluid Science*, 27(2), 2003, 177-186.
- [5] Moradi, A., Khodadadiyan, S., Study of real gas behavior in a single-stage gas gun, *International Journal of Mechanical and Mechatronics Engineering*, 78, 2011, 83-87.
- [6] Hamamoto, N., Kawazoe, H., Nakamura, Y., Arai, N., Kitagawa, K., Spectroscopic study of high enthalpy flow around a blunt body in arc-heated wind tunnel, *Energy Conversion and Management*, 38(10-13), 1997, 1177-1186.
- [7] Stalker, R., Plumb, D., Diaphragm-type Shock Tube for High Shock Speeds, *Nature*, 218, 1968, 789-790.




- [8] Smy, P., Electromagnetic Shock Tube capable of producing a Well-formed shock Wave of Low Attenuation, *Nature*, 193, 1962, 969-970.
- [9] Drummond, L., Exothermic Reactions behind a Reflected Shock, *Nature*, 216, 1967, 787-789.
- [10] Itoh, K., Ueda, S., Tanno, H., Komuro, T., Sato, K., Hypersonic aerothermodynamic and scramjet research using high enthalpy shock tunnel, *Shock Waves*, 12, 2002, 93-98.
- [11] Al-Falahi, A., Yusoff, M.Z., Ahmed, D.I., Shuaib, N.H., Experimental performance evaluation of short duration high speed flow shock tunnel, 3rd International Conference on Energy and Environment (ICEE), Malacca, Malaysia, 2009.
- [12] Stollery, J. Stagnation Temperature Measurements in a Hypersonic Wind-Tunnel using the Sodium Line Reversal Method, *Nature*, 190, 1961, 778-779.
- [13] Trivedi, S., Menezes, V., Measurement of yaw, pitch and side-force on a lifting model in a hypersonic shock tunnel, *Measurement*, 45(7), 2012, 1755-1764.
- [14] Yu, M.S., Heat Transfer by Shock-wave/boundary Layer Interaction on a Flat Surface with a Mounted Cylinder, *International Journal of Heat and Mass Transfer*, 55, 2012, 1764-1772.
- [15] Pennelegion, L., A Microwave Method of determining the Displacement and Velocity of a Piston in a Hypersonic Gun Tunnel, *Nature*, 183, 1959, 246.
- [16] Askari, S., An analytical approach for stand-off distance of detached shock waves, *Aerospace Science and Technology*, 28(1), 2013, 384-390.
- [17] Diyar, I.A., Al-Falahi, A., Yusoff, M.Z., Shuaib, N.H., Two dimensional numerical investigations on the velocity profile in a shock tunnel, *European Journal of Scientific Research*, 45(3), 2010, 458-469.
- [18] Vadassery, P., Joshi, D.D., Rolim, T.C., Lu, F.K., Design and Testing of an External Drag Balance for a Hypersonic Shock Tunnel, *Measurement*, 46(7), 2013, 2110-2117.
- [19] Banerjee, A., Analysis of shock waves over novel supersonic aircraft profiles using shadowgraph, *IEEE Aerospace Conference*, Big Sky, MT, USA, 2010.
- [20] Belcher, B., Measurement of the Effects of Piston Mass and Bursting Pressure on the Motion of a Piston in a Hypersonic Gun Tunnel, *Nature*, 184, 1959, 1207-1209.
- [21] Mallinson, S., Hillier, R., Jackson, A., Ki, D., Gun tunnel flow calibration: defining input conditions for hypersonic flow computations, *Shock Waves*, 10, 2000, 313-322.
- [22] Edney, E., Temperature Measurements in a Hypersonic Gun Tunnel Using Heat Transfer Methods, *Journal of Fluid Mechanics*, 27(3), 1967, 503-512.
- [23] Mohsen, A.M., Yusoff, M.Z., Hasini, H., Al-Falahi, A., Two-dimensional computational modeling of high-speed transient flow in gun tunnel, *Shock Waves*, 28(2), 2018, 335-348.
- [24] Sheng, Y., Liu, J., A computational technique for high enthalpy shock tube and shock tunnel flow simulation, *Shock Waves*, 8, 1998, 203-214.
- [25] Jacobs, P., Quasi-one-dimensional modeling of a free-piston shock tunnel, *AIAA Journal*, 32(1), 1994, 137-145.
- [26] Misawa, T., Ogawa, H., Fujiwara, T., Numerical analysis of viscous, Nonequilibrium, hypervelocity flow induced by a free piston shock tunnel, 21st International Symposium on Shock Waves, Great Keppel Island, Australia, 1997.
- [27] Peng, Y., Gerdroodbary, M.B., Sheikholeslami, M., Shafee, A., Babazadeh, H., Moradi, R., Mixing enhancement of the multi hydrogen fuel jets by the backward step, *Energy*, 203, 2020, 1-9.
- [28] Al-Falahi, A., Yusoff, M.Z., Yusaf, T., Numerical simulation of inviscid transient flows in shock tube and its validations, *International Journal of Mechanical, Aerospace, Industrial and Mechatronics Engineering*, 2(7), 2008, 1-11.
- [29] Al-Falahi, A., Yusoff, M.Z., Yusaf, T., Numerical and Experimental Study to Evaluate the Performance of Universiti Tenaga Nasional Short Duration Hypersonic Test Facility, 16th Australasian Fluid Mechanics Conference, School of Engineering, The University of Queensland, Australia, 2007.
- [30] Mohsen, A.M., Yusoff, M.Z., Al-Falahi, A., Shuaib, N.H., The Effects of Area Contraction on Shock Wave Strength and Peak Pressure in Shock Tube, *International Journal of Automotive and Mechanical Engineering*, 5, 2012, 587-596.
- [31] Mohsen, A.M., Yusoff, M.Z., Al-Falahi, A., Area Contraction Effect on Shock Tube Performance, Numerical and Experimental Study, *Journal of Engineering and Applied Sciences*, 10(20), 2015, 9614-9620.
- [32] Andreotti, R., Colombo, M., Guardone, A., Martinelli, P., Riganti, G., Prisco, M., Performance of a shock tube facility for impact response of structures, *International Journal of Non-Linear Mechanics*, 72, 2015, 53-66.
- [33] Kotov, Yee, H., Panesi, M., Prabhu, D., Wray, A., Computational challenges for simulations related to the NASA electric arc shock tube (EAST) experiments, *Journal of Computational Physics*, 269, 2014, 215-233.
- [34] Mundt, Boyce, R., Jacobs, P., Hannemann, K., Validation study of numerical simulations by comparison to measurements in piston-driven shock-tunnels, *Aerospace Science and Technology*, 11(2), 2007, 100-109.
- [35] Liou, M.S., Wada, Y., An accurate and robust flux splitting scheme for shock and contact discontinuities, *SIAM Journal on Scientific Computing*, 18, 1997, 633-657.
- [36] Warming, R.F., Beam, R.M., Upwind second order difference schemes and applications in aerodynamic flows, *AIAA Journal*, 14(9), 1976, 1242-1249.
- [37] VanLeer, B., Towards the ultimate conservative difference scheme vs a second order sequel to godunov's sequel, *Journal of Computational Physics*, 32, 1979, 101-136.
- [38] Lamnaouer, M., Numerical modeling of the shock tube flow fields before and during ignition delay time experiments at practical conditions, Ph.D. Thesis, University of Central Florida Orlando, 2010.
- [39] Kryukov, I.A., Ivanov, I.E., Shock wave - boundary layer interaction in a long shock tube, *IOP Conf. Series: Journal of Physics: Conf. Series*, Moscow, Russian Federation, 1009- 012010, 2010.
- [40] Musgrove, P.J., Appleton, J.P., The influence of boundary layer growth on shock tube test times, *Applied Scientific Research*, 18, 1968, 116-155.
- [41] Hideyuki, T., Tomoyuki, K., Kazuo, S., Katsuhiro, I., Free-flight force measurement technique in the impulsive facility HIEST, 22nd International Congress on Instrumentation in Aerospace Simulation Facilities, Pacific Grove, CA, USA, 2007.
- [42] Robinson, M.J., Meet, D.J., Three-Component Force Measurements on a Large Scramjet in a Shock Tunnel, *Journal of Spacecraft and Rockets*, 41(3), 2004, 416-425.
- [43] Wang, Y., Hu, Z., Liu, H., Jiang, Z., Starting Process in a Large-Scale Shock Tunnel, *AIAA Journal*, 54(4), 2016, 1240-1249.
- [44] Robinson, M.J., Schramm, J.M., Hannemann, K., An internal stress wave force balance for use in a shock tunnel, *Record International Congress on Instrumentation in Aerospace Simulation Facilities*, 2005, 100-109.


ORCID iD

A. M. Mohsen  <https://orcid.org/0000-0003-4253-8063>

M. Z. Yusoff  <https://orcid.org/0000-0001-8262-8165>

Hakim S. Sultan Aljibori  <https://orcid.org/0000-0002-5815-8148>

A. Al-Falahi  <https://orcid.org/0000-0002-0600-3603>

Abdul Amir H. Kadhum  <https://orcid.org/0000-0001-7140-6815>



© 2021 by the authors. Licensee SCU, Ahvaz, Iran. This article is an open access article distributed under the terms and conditions of the Creative Commons Attribution-NonCommercial 4.0 International (CC BY-NC 4.0 license) (<http://creativecommons.org/licenses/by-nc/4.0/>).

How to cite this article: A.M. Mohsen, M.Z. Yusoff, H.S. Sultan Aljibori, A. Al-Falahi, A.A.H. Kadhum, Two-Dimensional Numerical Study of the Transient Flow Conditions in Complete Shock Tunnel, *J. Appl. Comput. Mech.*, 7(2), 2021, 956-964. <https://doi.org/10.22055/JACM.2021.35491.2665>

